JACS
JOURNAL OF THE AMERICAN CHEMICAL SOCIETY
Article
pubs.acs.org/JACS

Kinetics and Low Temperature Studies of Electron Transfers in Films of Small (<2 nm) Au Monolayer Protected Clusters

Tessa M. Carducci and Royce W. Murray*

Department of Chemistry, Kenan Laboratories, The University of North Carolina at Chapel Hill, Chapel Hill, North Carolina 27599, United States

Supporting Information

ABSTRACT: This work examines the temperature dependence of electron transfer (ET) kinetics in solid-state films of mixed-valent states of monodisperse, small (<2 nm) Au monolayer protected clusters (MPCs). The mixed valent MPC films, coated on interdigitated array electrodes, are $Au_{25}(SR)_{18}^{0/1-}$, $Au_{25}(SR)_{18}^{1+/0}$, and $Au_{144}(SR)_{60}^{1+/0}$, where SR = hexanethiolate for Au_{144} and phenylethanethiolate for Au_{25}. Near room temperature and for ca. 1:1 mol:mol mixed valencies, the bimolecular ET rate constants (assuming a cubic lattice model) are $\sim 2 \times 10^6$ M^{-1} s^{-1} for $Au_{25}(SR)_{18}^{0/1-}$, $\sim 3 \times 10^5$ M^{-1} s^{-1} for $Au_{25}(SR)_{18}^{1+/0}$, and $\sim 1 \times 10^8$ M^{-1} s^{-1} for $Au_{144}(SR)_{60}^{1+/0}$. Their activation energy ET barriers are 0.38, 0.34, and 0.17 eV, respectively. At lowered temperatures (down to ca. 77 K), the thermally activated (Arrhenius) ET process dissipates revealing a tunneling mechanism in which the ET rates are independent of temperature but, among the different MPCs, fall in the same order of ET rate: $Au_{144}^{+1/0} > Au_{25}^{0/1-} > Au_{25}^{1+/0}$.

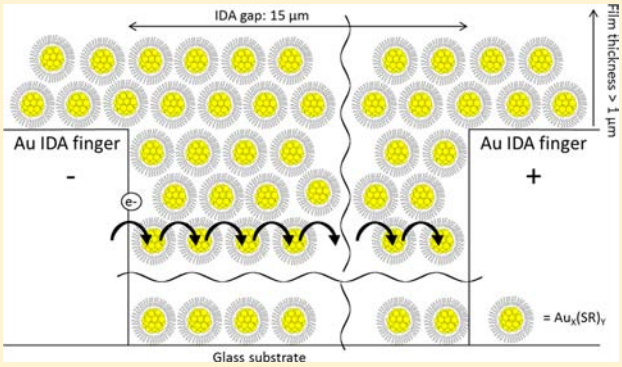

INTRODUCTION

Understanding the physical and chemical properties of nanoscale materials is a contemporary part of nanoparticle science. The appearance of altered properties when the dimensions of a material are diminished from the macro- to the nanoscale is sometimes referred to as the quantum confinement effect, and at its lower limit, characteristics arise that are associated with molecules, such as HOMO−LUMO gaps.[1] Nanoparticle properties are additionally influenced by capping ligands, such as Au nanoparticles coated with thiolate monolayers called monolayer protected clusters (MPCs).[2] In special cases, intermediate sizes of MPCs can exhibit electrochemical properties called quantized double layer charging (QDL).[3−5]

Among the research reports on electron transfers (ET) between Au MPCs, most have dealt with MPCs in a solvent-wetted state[6−14] and fewer with Au MPC ETs in a solvent-dry state[15−31] or at temperatures below 200 K.[32−42] The present work departs from most previous studies of ETs by using highly monodisperse samples of Au MPCs of, or approaching, molecular size[1] and characterizing their ET kinetics in dry (solvent-free), amorphous films containing set proportions of donors and acceptors. Utilizing the core-charging voltammetry of highly monodisperse small Au MPC solutions, solid-state films containing known states of electronic charging of the MPC cores can be prepared. In such dry films, ET reactions between MPCs can be induced under mild applied voltage gradients to exhibit linear current−voltage characteristics. Such measurements effectively yield solid-state MPC film conductivities sensitive to their mixed valent state (such as a 1:1 mixed valent state, abbreviated $MPC^{(Z+1)/Z}$). The corresponding solid-state electron self-exchange rates are the experimental topic of this paper, with special emphasis on how their rates change over a wide span of temperature (e.g., from room temperature down to 77 K).

For this work, we selected two size-purified 1−2 nm diameter Au MPCs: $Au_{144}(SR)_{60}$ (d_{core} = 1.6 nm)[15] and $Au_{25}(SR)_{18}$ (d_{core} = 1.0 nm)[43] that were prepared in roughly 1:1 mixed valent states of core charging, (e.g., $Au_{144}(SR)_{60}^{1+/0}$, $Au_{25}(SR)_{18}^{0/1-}$, and $Au_{25}(SR)_{18}^{1+/0}$). For the Au_{144} nanoparticle, SR is $-S(CH_2)_5CH_3$, and for the Au_{25} nanoparticle, SR is $-S(CH_2)_2Ph$. The mixed valent nanoparticle films were prepared by drop-casting their deaerated mixed valent solutions onto interdigitated array electrodes (IDA) so that the MPC film thicknesses exceed the IDA finger heights. Voltage biases applied to the IDA finger pairs supply the voltage gradient impetus for electron hopping within the dry, mixed valent nanoparticle films. For notational simplicity, the MPCs will be referred to as $Au_{25}^{0/1-}$, $Au_{25}^{1+/0}$, and $Au_{144}^{1+/0}$.

Previous electronic conductivity studies of Au MPC films of small, but not highly monodisperse, core sizes (Au_{25}[3,44,45] to Au_{976}) with alkanethiol ligand shells[15,17,46−48] were suggested to involve an ET pathway along the ligand chain to progress from Au core to core.[46] This process, illustrated in Figure 1, is

Received: May 28, 2013
Published: July 19, 2013

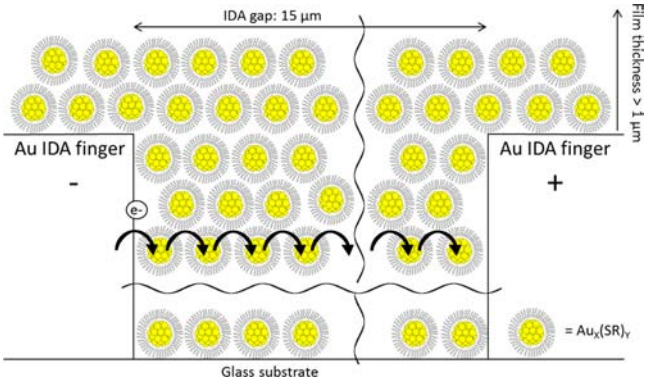

Figure 1. Cartoon of electron hopping conductivity in mixed-valent Au MPC film on an IDA electrode.

equivalent to a bimolecular electron "self-exchange" between MPCs according to[15]

$$MPC^{Z} + MPC^{Z+1} \overset{k_{EX}}{\leftrightarrow} MPC^{Z+1} + MPC^{Z} \quad (1)$$

where k_{EX} is the bimolecular nanoparticle electron self-exchange rate constant (M^{-1} s^{-1}). As with any bimolecular process, the ET rate and corresponding electronic conductivity, σ_{EL} (Ω^{-1} cm^{-1}), are maximized when $[MPC^{Z+1}] = [MPC^{Z}]$. Electronic conductivity in a sample of univalent MPCs (e.g., containing 100% of the neutral species, MPC^{0}) would proceed via self-exchange between charge carriers thermally generated by disproportionation. The disproportionation pathway is relatively unimportant for Au MPCs having a significant potential spacing between sequential-charge-state couples,[17] as in Au_{144} and Au_{25}.

This study expands on previous work at ambient temperatures by using more monodisperse syntheses of $Au_{144}^{1+/0}$ and $Au_{25}^{0/1-}$ nanoparticles and by looking at ET kinetics in the $Au_{25}^{1+/0}$ redox couple in addition to $Au_{25}^{0/1-}$. Most importantly, we further examine electronic conductivity in Au MPC films at cryogenic temperatures. Non-Arrhenius ET behavior at low temperatures was previously observed by our group[49] in films of mixed-valent osmium bipyridine polymers and by the Dhirani[33−36,42] group in much larger, polydisperse Au nanoparticles, as examples. At ambient temperatures, the greater occupancy of the upper vibrational states allows the reaction to proceed over the classical thermal barrier, whereas with decreasing temperature, the reaction is hypothesized to proceed increasingly by tunneling because of the depletion of the upper vibrational states.[50,51] In the present case, highly monodisperse, small Au MPC ETs in mixed-valent films at low temperatures unsurprisingly do not conform to a vibronic model and are instead treated simply as a transition from ET occurring predominantly over the classical thermal activation energy barriers to temperature-independent rates for electron tunneling at low temperatures.

EXPERIMENTAL SECTION

Materials. Hydrogen tetrachloroaurate(III) trihydrate ($HAuCl_4{\cdot}3H_2O$) was synthesized according to the literature.[52,53] 1-Hexanethiol ($C_6H_{13}SH$, 95%), 2-phenylethanethiol ($HSPh(CH_2)_2SH$ 98%), sodium borohydride ($NaBH_4$, 99%), and tetraoctylammonium bromide (Oct_4NBr, 98%) were purchased from Sigma-Aldrich (St. Louis, MO), tetrabutylammonium perchlorate (Bu_4NClO_4, 99.0%) was from Fisher Scientific (Suwanee, GA) or Fluka (Milwaukee, WI), and toluene (certified ACS reagent), methanol (optima grade), acetonitrile (CH_3CN, optima grade), and dichloromethane (CH_2Cl_2, optima grade) were from Fisher Scientific. Ethanol (absolute, i.e., 200 proof) was purchased from Pharmco-Aaper (Shelbyville, KY) or Decon Laboratories, Inc. (King of Prussia, PA). All chemicals were used without further purification. Nanopure water (resistance >18 MΩ) was prepared with a Thermo Scientific Barnstead Nanopure ultrapure water purification system.

Synthesis of Au MPCs. The syntheses[5,54] of $Au_{144}(SC_6H_{13})_{60}$ and $Au_{25}(SC_2Ph)_{18}$ as monodisperse nanoparticles are described in the Supporting Information in greater detail than previously reported.

Characterization of Au MPCs. The monodispersity of synthesized Au_{144} and Au_{25} nanoparticles were confirmed though voltammetry using a Pine WaveNano USB Potentiostat as illustrated by the differential pulse voltammetry patterns of Figure 2. QDL charging with uniformly spaced peaks is observed in the voltammetry for Au_{144},[5] whereas Au_{25}[55] nonoparticles display their known HOMO level doublet of peaks. The UV−visible spectrum (data not shown) of $Au_{25}(SC_2Ph)_{18}$ was obtained using a Thermo Evolution Array UV−

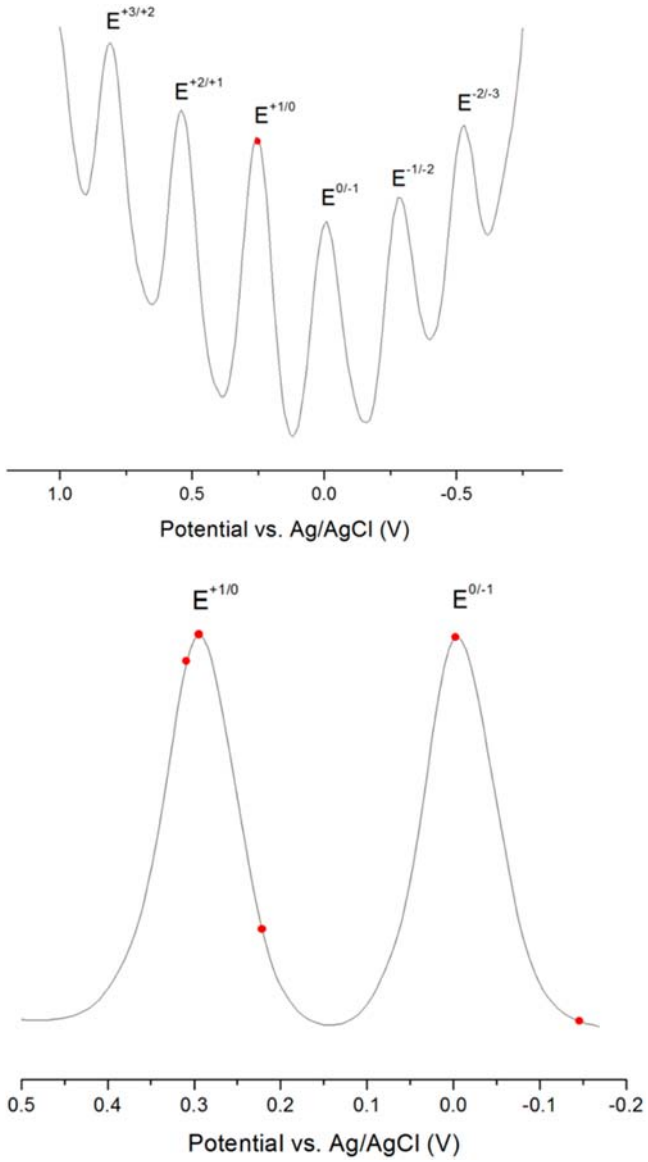

Figure 2. (Top) Differential pulse voltammetry (DPV) of ∼1 mM $Au_{144}(SC_6H_{13})_{60}$ in 0.1 M Bu_4NClO_4/CH_2Cl_2 at 0.020 cm^2 Pt disk. Points in red are rest potentials of solutions from which mixed valent MPC samples were isolated. (Bottom) DPV of ∼1 mM $Au_{25}(SC_2Ph)_{18}$ in 0.1 M Bu_4NClO_4 in CH_2Cl_2. Data taken with a Pine WaveNano USB potentiostat.

dx.doi.org/10.1021/ja405342r | J. Am. Chem. Soc. 2013, 135, 11351−11356

visible spectrophotometer. All expected characteristic spectral features[54] were observed.

Preparation of Mixed-Valent Au MPCs. Bulk electrolysis of Au MPCs was performed in a fine frit-separated, three-compartment cell, using a Pine WaveNow USB potentiostat. The electrolysis was aimed to acquire Au MPC samples with known mixed valencies, especially near 1:1 mol ratios (e.g., $Au_{144}^{1+/0}$, $Au_{25}^{0/1-}$, and $Au_{25}^{1+/0}$). We chose electrolysis potentials (E_{elec}) based on Nernst equation[56,57] with reference to known MPC voltammetry

$$E_{elec} - E^{(Z+1)/Z} = 0.059 \log \frac{[MPC^{Z+1}]}{[MPC^{Z}]} \quad (2)$$

where $E^{(Z+1)/Z}$ was determined by DPV of the Au MPCs. The working electrode was a Pt gauze (Sigma-Aldrich) and was placed with the reference electrode in cell compartment 1, with the Pt counter electrode in compartment 3. In preparing mixed-valent samples of Au_{144}, compartment 1 contained ~10 mL of 1 mM Au_{144} in CH_2Cl_2 plus 10 mM Bu_4NClO_4 as supporting electrolyte. Compartments 2 and 3 contained only 10 mM Bu_4NClO_4/CH_2Cl_2. In preparing mixed-valent Au_{25} nanoparticles, compartment 1 contained ~10 mL of 1 mM Au_{25} plus 1 mM Bu_4NClO_4 in CH_2Cl_2. Compartments 2 and 3 contained only 1 mM Bu_4NClO_4/CH_2Cl_2. All cells were stirred and degassed with dichloromethane-saturated Ar. When the electrolysis current dropped to ~1% of the initial value, the electrolysis was stopped and the open circuit potential was checked.

Following bulk electrolysis, the Au MPC sample solution was thoroughly degassed again and its open circuit potential vs Ag/AgCl reference determined at a clean Pt wire, using a Keithley Instruments 610C solid-state electrometer (input impedance $>10^8$ MΩ). The MPC charge-state distribution was calculated from the rest potential and the DPV-determined formal potentials according to eq 2.

Mixed-valent samples of Au_{144} were washed twice with CH_3CN following bulk electrolysis to remove excess electrolyte. The wash steps did not alter the open circuit potential. Samples of Au_{25} were not washed because the used electrolyte concentration was only 1 mM.

Film Preparation on Interdigitated Array Electrodes. IDAs (microfabricated in-house by the Chapel Hill Analytical and Nuclear Laboratory, CHANL) had 50 interdigitated Au fingers on a glass substrate. IDAs made for Au_{144} measurements had 0.298 cm long fingers spaced 15 μm apart. IDAs made for Au_{25} samples had 50 interdigitated fingers (0.298 cm long) spaced 10 μm apart; the smaller IDA gap was chosen to increase currents in the conductivity scans. Connections to finger sets were made with soldered wire leads covered with epoxy resin. Films of Au MPCs were drop-cast onto the IDA electrodes from concentrated Au MPC toluene solutions, ~10 mg in one small drop. Au_{144} MPC concentrations in the solid-state films were 0.07 M based on pycnometry. Au_{25} was 0.17 M as determined previously[17] by UV–visible spectroscopy. IDA electrodes were rinsed thoroughly, but gently, with CH_2Cl_2 and plasma-cleaned between uses.

Low Temperature Conductivities of Solid-State Au MPC Films. Temperatures of Au MPC films were controlled using a Janus VPF 100 liquid nitrogen cryostat system and Lakeshore 331S temperature controller. IDAs with drop-cast Au MPC films were secured to the heat-conducting sample stage of the cryostat using double sided tape. The cryostat chamber was evacuated overnight using an Edwards RV8 rotary vane pump, which is required for proper function of the temperature controls and to ensure complete drying of the MPC films. The cryostat cooling chamber was filled with liquid nitrogen and allowed to cool to the minimum temperature (~77 K) prior to initiation of electronic conductivity measurements of solid-state mixed-valent Au MPC films. Measurements were done using a home-built two-electrode circuit designed for applying a voltage ramp and measuring currents as low as 10^{-10} A (controlled by LabView software). Capacitance was minimized by connecting the circuit directly to the cryostat. Electronic conductivities were calculated from the slopes of current–potential plots in the linear potential bias interval from −0.25 to +0.25 V (initial and final voltage is 0 V). The scan rate was 10 V/s, a rate aimed at avoiding ion migration within the film. As an additional caution against electrostatic migration of counterions of the mixed valent film and its consequent electrolysis, conductivity measurements were not performed above 300 K. Conductivity scans were performed at temperature intervals between 2 and 10 K as the IDA electrode was heated in a controlled manner from 77 to 300 K.[58]

The mixed valent MPC film electronic conductivity, σ_{EL}, was calculated from the slopes of the current–potential plots according to[15,17]

$$\sigma_{EL} = \left(\frac{d}{A_{total}}\right)\frac{\Delta i}{\Delta E} \quad (3)$$

where d is the IDA gap, A_{total} is the area of the walls (A_{finger}) of facing parallel plate finger electrodes, of height taken as the maximum conductive MPC film thickness (ca. 1 μm), and length equal to the finger length times $N - 1$, where N is the total number of fingers (50). (Note that the current of each interior finger is double that of an end finger.) The ratio d/A_{total} comprises the geometric cell constant, C_{cell}, which for the IDAs used for Au_{144} films was 1.021 cm^{-1} and for Au_{25} films was 0.685 cm^{-1}.

RESULTS AND DISCUSSION

Electronic Conductivity of Au MPC Films from 77 to 300 K Temperatures. Electronic conductivity results for Au MPC films from 77 to 300 K are presented in Figures 3 and 4

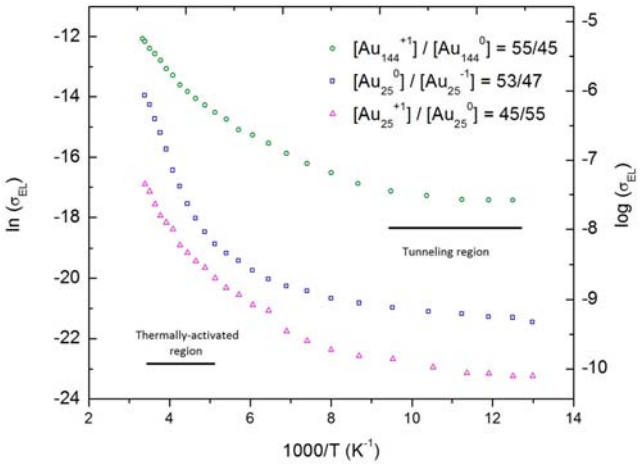

Figure 3. Arrhenius plot of mixed valent solid-state Au MPC films containing indicated molar proportions of each MPC charge-state.

as Arrhenius plots. The data can be divided into two regimes of behavior; higher temperatures display thermally activated ET (electron hopping) and strongly temperature-dependent rates, whereas at lower temperatures, the ET conductivity becomes temperature-independent, which is characteristic of electron tunneling. To our knowledge, the latter is the first report of nanoparticle-to-nanoparticle electron tunneling in 1–2 nm Au MPCs.

In the thermally activated ET region at higher temperatures, the relevant relation is[46]

$$\ln(\sigma_{EL}) = \frac{-E_A}{RT} - r_0\beta + \ln \sigma_0 \quad (4)$$

where β (cm^{-1}) is an electronic coupling term[46] for ET tunneling through the MPC organothiolate ligand shell and γ_0 (cm) is the average edge-to-edge distance between neighboring MPC Au cores. The y-intercept represents the equivalent of an infinite-temperature electronic conductivity.[15,46] The activation energy barrier (E_A) to ET in the Au MPC films was taken from

dx.doi.org/10.1021/ja405342r | J. Am. Chem. Soc. 2013, 135, 11351–11356

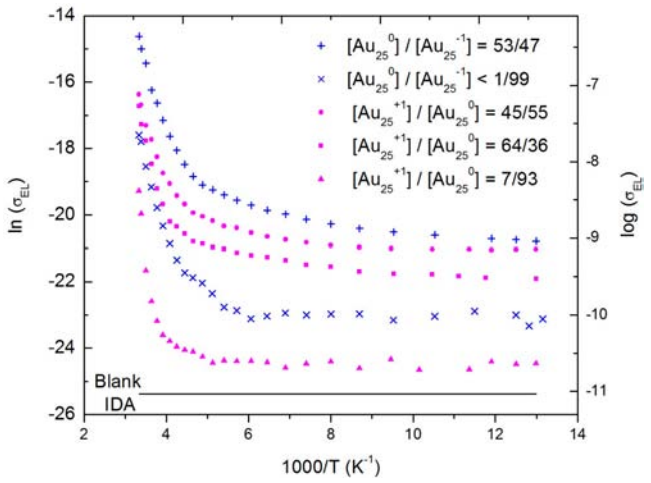

Figure 4. Arrhenius plots of mixed valent solid-state Au_{25} MPC films containing the indicated proportions of the 0/1− or 1+/0 charge-states. The blank IDA line is for an IDA electrode bearing no MPC film.

the best-fit slopes over the data points taken at temperatures from 265 to 300 K.

Figures 3 and 4 show that the transition between thermally activated and tunneling ET behavior is gradual.[49,51] In any redox system, the current measured at any given temperature can be expressed as the sum of currents arising from all ET pathways.[51] In the flattened, low temperature regions of the Arrhenius plots of Figures 3 and 4, the ET conductivity arises solely through the mechanism of tunneling. The tunneling current dominates at low temperatures as energy-activated states become irrelevant; thermal energy is depleted and electron hopping diminished. In the thermally activated region, the electron hopping mechanism dominates, and tunneling current becomes a minor contributor because it retains its small value regardless of temperature.

In a previous study,[49] we assessed tunneling parameters for low temperature ET in mixed-valent osmium bipyridine polymers using the Holstein[59] equation. In the present case, we were unable to produce satisfactory fits to the data in Figures 3 and 4. We conclude that the vibronic Holstein model is not an appropriate one for the present experiments and a classical tunneling description instead.

The limiting values of the temperature-independent conductivities (near 77 K) were not very reproducible (uncertainty ca.±67%), but some semiquantitative observations about the efficacy of electron tunneling for the different Au MPC samples are possible. From Figure 3, the electron tunneling current appears to be core-size-dependent; that for Au_{144} MPCs is greater than that for Au_{25}. This difference occurs in spite of the difference in nanoparticle ligand; those of the Au_{25} nanoparticles are partly aromatic. Second, the $Au_{25}L_{18}^{1+/0}$ data in Figure 4 indicate that the tunneling currents are largest for MPC samples with mixed valency nearest 1:1. Third, the effect of core size is larger than that of mixed valent proportions within a given redox couple (Figure 3). Finally, the low temperature tunneling currents for mixed-valent $Au_{25}^{0/1-}$ exceed those for $Au_{25}^{+1/0}$. These trends in the tunneling currents largely mimic those of conductivities at higher temperatures[60] discussed further in the next section.

E_A and σ_{EL} Measurements in the Thermally Activated Region. Table 1 presents values of E_A and σ_{EL} (at T = 298 K) for the different Au MPC redox couples. These values are averages from three different films with the same mixed valent composition. As noted in the Introduction, a significant difference in E_A and σ_{EL} for Au_{144} and Au_{25} has previously been reported.[17] This core size effect is also seen in the present data, which are for more highly monodisperse MPCs; E_A for Au_{25} is more than 2-fold larger than that for Au_{144}, and σ_{EL} is about 1 order of magnitude larger for $Au_{144}^{+1/0}$ than that of $Au_{25}^{0/1-}$. Possible origins of the increase in E_A and decrease in σ_{EL} for smaller core sizes of metal-based MPCs are an increase in density of states for larger particles[61] requiring a smaller Marcus inner-sphere reorganizational energy[17] and increased consequences of any Coulomb blockade-like phenomena.[62]

Previously reported[15,17] values of σ_{EL} for Au_{144} and $Au_{25}^{0/1-}$ MPCs were ca. 10^{-5} and 10^{-7} Ω^{-1} cm^{-1}, respectively. Differences in the present data are possibly related to differences in the degree of MPC monodispersity or to our improved method of cleaning of electrodes. Cleaning of IDA electrodes with piranha solution in previous studies produces some scattered damage to the Au fingers. The present cleaning procedure did not produce changes due to surface conductivity of the glass bottom of the IDA channels, as shown by a control experiment of an "empty" (no nanoparticle film) IDA; see the "blank" IDA result of Figure 4.

The present room temperature E_A and σ_{EL} data allow a comparison of the electronic conductivities of solid-state films of Au_{25} nanoparticles to the rates of electron transfers between dissolved Au_{25} nanoparticle couples. Solution voltammetry[63] of freely diffusing Au_{25} nanoparticles disclosed that ET was slower for the $Au_{25}^{1+/0}$ than that of the $Au_{25}^{0/1-}$, by about half an order of magnitude. This kinetic difference is also seen for the solid-state materials; the electronic conductivity in the solid-state $Au_{25}^{1+/0}$ couple was slower than that of the $Au_{25}^{0/1-}$ couple by about 1 order of magnitude.

The role of the counterion is a potentially significant component of the electronic conductivities of samples of mixed

Table 1. Activation Energy Barriers (E_A), Electron Hopping Conductivities (σ_{EL}), and Self-Exchange Rate Constant (k_{EX}) at 298 K of Solid-State, Mixed Valent Au MPC Films

MPC	$[MPC^{Z+1}]$ (%)	E_A (eV)	σ_{EL}(Ω^{-1} cm^{-1})	k_{EX} (M^{-1} s^{-1})
$Au_{144}^{+1/0}$	55[a]	0.17 ± 0.02	(5.9 ± 0.9) × 10^{-6}	(1.24 ± 0.19) × 10^{8}
$Au_{25}^{0/1-}$	53	0.38 ± 0.03	(6.3 ± 2.2) × 10^{-7}	(2.44 ± 0.86) × 10^{6}
	<1[b]	0.46 ± 0.02	(1.6 ± 0.7) × 10^{-8}	
$Au_{25}^{+1/0}$	45	0.34 ± 0.09	(6.4 ± 1.2) × 10^{-8}	(2.50 ± 0.47) × 10^{5}
	64	0.47 ± 0.07	(4.4 ± 3.1) × 10^{-8}	(1.8 ± 1.3) × 10^{5}
	7[b]	0.7 ± 0.1	(1.7 ± 1.2) × 10^{-9}	(2.6 ± 1.8) × 10^{4}

[a]Average of four different films having the same mixed valent composition. [b]Average of two different films having the same mixed valent composition.

dx.doi.org/10.1021/ja405342r | J. Am. Chem. Soc. 2013, 135, 11351−11356

valent $Au_{25}^{1+/0}$ MPCs relative to those of $Au_{25}^{0/1-}$ MPCs. Films of $Au_{25}^{0/1-}$ contain a counterion (Bu_4N^+ in the present case), whereas those of $Au_{25}^{1+/0}$ MPCs contain the counterion ClO_4^{1-}. What roles the choice of solid-state counterion play are unknown, whether benign observers or active participants in some way. Differences in the electrolyte may be responsible, for example, for the variation in E_A between the two redox-state pairs. Direct evidence, such as a study comparing $Au_{25}^{1+/0}$ and $Au_{25}^{0/1-}$ with varying electrolytes species present, is lacking at present and so this issue is unresolved.

Expression of Conductivity as Electron Self-exchange Rate Constants. We have previously expressed electronic conductivities of mixed valent Au MPCs as bimolecular electron self-exchange rate constants (k_{EX}) by assuming a cubic lattice film structure[8,15−17,64]

$$k_{EX} = \frac{6(10^3)RT\sigma_{EL}}{F^2\delta^2[MPC^{Z+1}][MPC^{Z}]} \quad (5)$$

where δ is the core-to-core edge separation (cm) and $[MPC^{Z+1}]$ and $[MPC^{Z}]$ are calculated from the Nernst equation. δ for Au_{144} was previously estimated as 2.5 nm, from transmission electrom microscopy (TEM) images showing a core diameter of 1.6 nm,[65] to which was added 0.15 nm per $-CH_2$ of the hexanethiolate ligand.[15] On the basis of the model, for Au_{25}, δ was estimated[17] as 2.4 nm

$$\delta_{Au_{25}} = 2r_{core} + l_{eff} = 2\left(\frac{(0.7)(10^3)}{\frac{4}{3}\pi C_{film}N_{Avo}}\right)^{1/3} \quad (6)$$

where r_{core} is Au_{25} MPC core radius, l_{eff} is the ligand-separated distance between two cores, C_{film} is the mol/cm^3 MPC concentration, and 0.7 is a hexagonal packing fill factor. C_{film} was taken as 0.17 M for Au_{25}, as determined through UV−visible absorption spectroscopy[17] and 0.07 M for Au_{144} determined through pycnometry (see Experimental Section). The value of δ estimated for Au_{144} suggests almost complete interdigitation of the ligands of neighboring particles, whereas the calculated value for Au_{25} suggests no ligand interdigitation. In recent density functional theory calculations, Lopez-Acevedo et al.[66] estimated the Au_{144} core radius as 8 Å, in agreement with TEM measurements. Heaven et al.[43] reported the crystal structure of the Au_{25} MPC and the diameter was 2.39 nm, which is close to the above result from a cubic lattice model. Thus, although the two diameters are nominally close, the data background indicates that $\delta_{Au_{144}}$ = 2.5 nm and $\delta_{Au_{25}}$ = 2.4 nm.

Our previous studies[15,17] showed that k_{EX} is maximized in films where $[MPC^{Z+1}] = [MPC^{Z}]$ in Au_{144} and $Au_{25}^{0/1-}$. The data in Table 1 (last column) for mixed valent $Au_{25}^{1+/0}$ are consistent with these observations and also show that k_{EX} for mixed valent $Au_{25}^{1+/0}$ is ca. 10-fold smaller than that of the $Au_{25}^{1+/0}$ couple (like the σ_{EL} difference). Having no basis to assume a difference from $Au_{25}^{0/1-}$, we use the same value of δ for $Au_{25}^{0/1-}$ and $Au_{25}^{1+/0}$ to calculate k_{EX}.

In summary, we find that electron transfer rates in mixed valent films of monodisperse $Au_{25}(SC_2Ph)_{18}$ and $Au_{144}(SC_6H_{13})_{60}$ nanoparticles can be observed over a complete range of thermal activation of electron hopping to temperature-independent rates of electron hopping at lowered temperatures. The electron hopping rates at lowered temperatures fall in the order $Au_{144}^{1+/0} > Au_{25}^{0/1-} > Au_{25}^{1+/0}$.

■ ASSOCIATED CONTENT

Supporting Information

More detailed information about $Au_{25}(SC_2Ph)_{18}$ and $Au_{144}(SC_6H_{13})_{60}$ syntheses and a schematic of the IDA electrode. This material is available free of charge via the Internet at http://pubs.acs.org.

■ AUTHOR INFORMATION

Corresponding Author

rwm@email.unc.edu

Notes

The authors declare no competing financial interest.

■ ACKNOWLEDGMENTS

The authors thank Stephen W. Feldberg and Norman Sutin of Brookhaven National Laboratories for insightful comments during the course of this work, Collin McKinney and Matt Verber of the UNC Electronics Facility for conductivity circuit design, and Bob Geil of CHANL for microfabricating IDA electrodes. This work was supported by the Office of Naval Research. T.C. acknowledges support from a National Defense Science & Engineering Graduate (NDSEG) Fellowship, from the Department of Defense.

■ REFERENCES

(1) Chen, S.; Ingram, R. S.; Hostetler, M. J.; Pietron, J. J.; Murray, R. W.; Schaaff, T. G.; Khoury, J. T.; Alvarez, M. M.; Whetten, R. L. *Science* **1998**, *280*, 2098.
(2) Sardar, R.; Funston, A. M.; Mulvaney, P.; Murray, R. W. *Langmuir* **2009**, *25*, 13840.
(3) Murray, R. W. *Chem. Rev.* **2008**, *108*, 2688.
(4) Chen, S.; Murray, R. W.; Feldberg, S. W. *J. Phys. Chem. B* **1998**, *102*, 9898.
(5) Hicks, J. F.; Miles, D. T.; Murray, R. W. *J. Am. Chem. Soc.* **2002**, *124*, 13322.
(6) Yang, Y.; Pradhan, S.; Chen, S. *J. Am. Chem. Soc.* **2004**, *126*, 76.
(7) Lee, W. Y.; Hostetler, M. J.; Murray, R. W.; Majda, M. *Isr. J. Chem.* **1997**, *37*, 213.
(8) Hicks, J. F.; Zamborini, F. P.; Osisek, A. J.; Murray, R. W. *J. Am. Chem. Soc.* **2001**, *123*, 7048.
(9) Kim, J.; Lee, D. *J. Am. Chem. Soc.* **2006**, *128*, 4518.
(10) Parker, J. F.; Choi, J. P.; Wang, W.; Murray, R. W. *J. Phys. Chem. C* **2008**, *112*, 13976.
(11) Li, W.; Su, B. *Electrochem. Commun.* **2012**, *22*, 8.
(12) Peterson, R. R.; Cliffel, D. E. *Langmuir* **2006**, *22*, 10307.
(13) Hicks, J. F.; Zamborini, F. P.; Murray, R. W. *J. Phys. Chem. B* **2002**, *106*, 7751.
(14) Brennan, J. L.; Branham, M. R.; Hicks, J. F.; Osisek, A. J.; Donkers, R. L.; Georganopoulou, D. G.; Murray, R. W. *Anal. Chem.* **2004**, *76*, 5611.
(15) Wuelfing, W. P.; Green, S. J.; Pietron, J. J.; Cliffel, D. E.; Murray, R. W. *J. Am. Chem. Soc.* **2000**, *122*, 11465.
(16) Wuelfing, W. P.; Murray, R. W. *J. Phys. Chem. B* **2002**, *106*, 3139.
(17) Choi, J. P.; Murray, R. W. *J. Am. Chem. Soc.* **2006**, *128*, 10496.
(18) Chen, S. *J. Mater. Chem.* **2007**, *17*, 4115.
(19) Pradhan, S.; Kang, X.; Mendoza, E.; Chen, S. *Appl. Phys. Lett.* **2009**, *94*, 042113/1.
(20) Pradhan, S.; Sun, J.; Deng, F.; Chen, S. *Adv. Mater.* **2006**, *18*, 3279.
(21) Chaki, N. K.; Singh, P.; Dharmadhikari, C. V.; Vijayamohanan, K. P. *Langmuir* **2004**, *20*, 10208.
(22) Chaki, N. K.; Kakade, B.; Vijayamohanan, K. P.; Singh, P.; Dharmadhikari, C. V. *Phys. Chem. Chem. Phys.* **2006**, *8*, 1837.
(23) Zamborini, F. P.; Smart, L. E.; Leopold, M. C.; Murray, R. W. *Anal. Chim. Acta* **2003**, *496*, 3.

(24) Suganuma, Y.; Trudeau, P. E.; Dhirani, A. A. *Phys. Rev. B: Condens. Matter Mater. Phys.* **2002**, *66*, 241405/1.
(25) Suganuma, Y.; Trudeau, P. E.; Dhirani, A. A.; Leathem, B.; Shieh, B. *J. Chem. Phys.* **2003**, *118*, 9769.
(26) Chen, S.; Xu, L. P.; Pradhan, S.; Chen, W. *Solid State Commun.* **2007**, *144*, 124.
(27) Wang, G. R.; Wang, L.; Rendeng, Q.; Wang, J.; Luo, J.; Zhong, C. J. *J. Mater. Chem.* **2007**, *17*, 457.
(28) Wang, W.; Lee, D.; Murray, R. W. *J. Phys. Chem. B* **2006**, *110*, 10258.
(29) Lee, D.; Donkers, R. L.; DeSimone, J. M.; Murray, R. W. *J. Am. Chem. Soc.* **2003**, *125*, 1182.
(30) Leopold, M. C.; Donkers, R. L.; Georganopoulou, D.; Fisher, M.; Zamborini, F. P.; Murray, R. W. *Faraday Discuss.* **2003**, *125*, 63.
(31) Zamborini, F. P.; Leopold, M. C.; Hicks, J. F.; Kulesza, P. J.; Malik, M. A.; Murray, R. W. *J. Am. Chem. Soc.* **2002**, *124*, 8958.
(32) Miles, D. T.; Murray, R. W. *Anal. Chem.* **2003**, *75*, 1251.
(33) Joanis, P.; Tie, M.; Dhirani, A. A. *Langmuir* **2013**, *29*, 1264.
(34) Dunford, J. L.; Suganuma, Y.; Dhirani, A. A.; Statt, B. *Phys. Rev. B: Condens. Matter Mater. Phys.* **2005**, *72*, 075441/1.
(35) Dunford, J. L.; Dhirani, A. A. *Nanotechnology* **2008**, *19*, 025202.
(36) Zabet-Khosousi, A.; Trudeau, P. E.; Suganuma, Y.; Dhirani, A. A.; Statt, B. *Phys. Rev. Lett.* **2006**, *96*, 156403/1.
(37) Suganuma, Y.; Dhirani, A. A. *J. Phys. Chem. B* **2005**, *109*, 15391.
(38) Trudeau, P. E.; Orozco, A.; Kwan, E.; Dhirani, A. A. *J. Chem. Phys.* **2002**, *117*, 3978.
(39) Trudeau, P. E.; Escorcia, A.; Dhirani, A. A. *J. Chem. Phys.* **2003**, *119*, 5267.
(40) Muller, K. H.; Herrmann, J.; Wei, G.; Raguse, B.; Wieczorek, L. *J. Phys. Chem. C* **2009**, *113*, 18027.
(41) Li, C. P.; Wu, C. H.; Wei, K. H.; Sheu, J. T.; Huang, J. Y.; Jeng, U. S.; Liang, K. S. *Adv. Funct. Mater.* **2007**, *17*, 2283.
(42) Zabet-Khosousi, A.; Dhirani, A. A. *Chem. Rev.* **2008**, *108*, 4072.
(43) Heaven, M. W.; Dass, A.; White, P. S.; Holt, K. M.; Murray, R. W. *J. Am. Chem. Soc.* **2008**, *130*, 3754.
(44) An initial mislabeling of the Au_{25} nanoparticle as Au_{38} was corrected by mass spectrometry in ref 45.
(45) Tracy, J. B.; Crowe, M. C.; Parker, J. F.; Hampe, O.; Fields-Zinna, C. A.; Dass, A.; Murray, R. W. *J. Am. Chem. Soc.* **2007**, *129*, 16209.
(46) Terrill, R. H.; Postlethwaite, T. A.; Chen, C. h.; Poon, C. D.; Terzis, A.; Chen, A.; Hutchison, J. E.; Clark, M. R.; Wignall, G. *J. Am. Chem. Soc.* **1995**, *117*, 12537.
(47) Snow, A. W.; Wohltjen, H. *Chem. Mater.* **1998**, *10*, 947.
(48) Pettibone, J. M.; Hudgens, J. W. *ACS Nano* **2011**, *5*, 2989.
(49) Jernigan, J. C.; Surridge, N. A.; Zvanut, M. E.; Silver, M.; Murray, R. W. *J. Phys. Chem.* **1989**, *93*, 4620.
(50) Sutin, N. In *Progress in Inorganic Chemistry: An Appreciation of Henry Taube*; Lippard, S. J., Ed.; John Wiley & Sons, Inc.: Hoboken, NJ, USA, 2007; Vol. *30*.
(51) McCreery, R. L. *Chem. Mater.* **2004**, *16*, 4477.
(52) Block, B. P.; Therald Moeller, S. A. B.; Chrisp, J. D.; Gentile, P.; and Morgan, L. O. In *Inorganic Syntheses*; Bailar, J. C., Ed.; McGraw-Hill Book Company, Inc.: New York, NY, 1953; Vol. *4*, p 14.
(53) Glemser, O.; Sauer, H. *Handbook of Preparative Inorganic Chemistry*, 2nd ed.; Brauer, G., Ed.; Academic Press: New York, 1963; Vol. *2*, p 1057.
(54) Parker, J. F.; Weaver, J. E. F.; McCallum, F.; Fields-Zinna, C. A.; Murray, R. W. *Langmuir* **2010**, *26*, 13650.
(55) Lee, D.; Donkers, R. L.; Wang, G.; Harper, A. S.; Murray, R. W. *J. Am. Chem. Soc.* **2004**, *126* (19), 6193−6199.
(56) Bard, A. J.; Faulkner, L. R. *Electrochemical Methods Fundamentals and Applications*, 2nd ed.; John Wiley & Sons: Hoboken, NJ, 2001.
(57) Pietron, J. J.; Hicks, J. F.; Murray, R. W. *J. Am. Chem. Soc.* **1999**, *121*, 5565.
(58) Temperature was always varied from low to high due to constraints of the cryostat. Repeat experiments on a given MPC film and IDA show no significant differences. All data reported are averages from different IDAs with different MPC films.
(59) Holstein, T. In *Tunneling in Biological Systems*; Britton Chance, R. A. M.; DeVault, Don Charles; Robert Schrieffer, J.; Frauenfelder, Hans; Sutin, Norman, Eds.; Academic Press: New York, NY, 1979, p 129.
(60) Normalizing for proportions of mixed valency beings the conductivity data together for high but not low temperatures.
(61) Guidez, E. B.; Aikens, C. M. *Phys. Chem. Chem. Phys.* **2012**, *14*, 4287.
(62) Chen, S. *J. Electroanal. Chem.* **2004**, *574* (1), 153−165.
(63) Antonello, S.; Holm, A. H.; Instuli, E.; Maran, F. *J. Am. Chem. Soc.* **2007**, *129*, 9836.
(64) Savéant, J. M. *J. Electroanal. Chem. Interfacial Electrochem.* **1988**, *242*, 1.
(65) Hostetler, M. J.; Wingate, J. E.; Zhong, C. J.; Harris, J. E.; Vachet, R. W.; Clark, M. R.; Londono, J. D.; Green, S. J.; Stokes, J. J.; Wignall, G. D.; Glish, G. L.; Porter, M. D.; Evans, N. D.; Murray, R. W. *Langmuir* **1998**, *14*, 17.
(66) Lopez-Acevedo, O.; Akola, J.; Whetten, R. L.; Grönbeck, H.; Häkkinen, H. *J. Phys. Chem. C* **2009**, *113*, 5035.